Research Article Vol. 15, No. 12 / 1 Dec 2024 / Biomedical Optics Express 6739
Biomedical Optics EXPRESS

Cerebral blood flow patterns induced by photoactivation based on laser speckle contrast imaging

XUAN ZHU,[1] LIANG SHI,[1] PENGCHENG LI,[1,2,3] AND JINLING LU[1,*]

[1]Britton Chance Center for Biomedical Photonics and MoE Key Laboratory for Biomedical Photonics, Advanced Biomedical Imaging Facility, Wuhan National Laboratory for Optoelectronics, Huazhong University of Science and Technology, Wuhan, Hubei 430074, China
[2]State Key Laboratory of Digital Medical Engineering, Key Laboratory of Biomedical Engineering of Hainan Province, School of Biomedical Engineering, Hainan University, Sanya 572025, China
[3]Research Unit of Multimodal Cross Scale Neural Signal Detection and Imaging, Chinese Academy of Medical Science, HUST-Suzhou Institute for Brainsmatics, JITRI, Suzhou 215100, China
*lujinling@mail.hust.edu.cn

Abstract: Neurovascular coupling (NVC) is crucial for maintaining brain function and holds significant implications for diagnosing neurological disorders. However, the neuron type and spatial specificity in NVC remain poorly understood. In this study, we investigated the spatiotemporal characteristics of local cerebral blood flow (CBF) driven by excitatory (VGLUT2) and inhibitory (VGAT) neurons in the mouse sensorimotor cortex. By integrating optogenetics, wavefront modulation technology, and laser speckle contrast imaging (LSCI), we achieved precise, spatially targeted photoactivation of type-specific neurons and real-time CBF monitoring. We observed three distinct CBF response patterns across different locations: unimodal, bimodal, and biphasic. While unimodal and bimodal patterns were observed in different locations for both neuron types, the biphasic pattern was exclusive to inhibitory neurons. Our results reveal the spatiotemporal complexity of NVC across different neuron types and demonstrate our method's ability to analyze this complexity in detail.

1. Introduction

Neurovascular coupling (NVC) is the process by which changes in local neuronal activity are coupled with changes in cerebral blood flow (CBF). Comprehending the impact of neuronal activity on CBF is extremely important for revealing brain function [1]. The brain vascular network is primarily responsible for delivering essential metabolic and respiratory substances to cells and removing harmful metabolic byproducts, thereby maintaining tissue survival and function. The regulation of CBF within the vascular network is largely influenced by the activation of nearby neurons, which are the most energy-demanding cells in the brain [2,3]. Understanding the mechanisms mediating NVC is essential for comprehending the pathway of brain information processing and the pathophysiology of neurological disorders where neurovascular coupling is disrupted [4].

NVC is a sophisticated process requiring coordinated interactions among diverse cell types to precisely align local CBF with the neural energy demands both spatially and temporally [2]. Optogenetics is a valuable method for studying NVC by using light to modulate type-specific neurons through light-sensitive ion channel proteins like channelrhodopsin2 (ChR2) [5–7]. Vazquez et al. demonstrated that optogenetic activation of pyramidal neurons expressing ChR2 led to an increase in CBF [8]. Anenberg et al., on the other hand, activated γ-aminobutyric acid (GABA) neurons with light and discovered that inhibitory neuronal activity can also lead

#541444 https://doi.org/10.1364/BOE.541444
Journal © 2024 Received 4 Sep 2024; revised 29 Oct 2024; accepted 30 Oct 2024; published 8 Nov 2024

Biomedical Optics EXPRESS

to an increase in CBF [9]. However, Moon et al. observed that under optogenetic stimulation, excitatory neurons elicited a positive blood oxygenation level-dependent (BOLD) response, while inhibitory neurons produced a biphasic response [10]. Uhlirova et al. selectively activated excitatory and inhibitory neuronal activities, which led to different vascular responses [11]. These studies highlight the diverse patterns of blood flow responses linked to different neuronal activities.

Additionally, due to the differing demands across various anatomical regions of brain, the vascular system exhibits spatial differences [12]. Gene expression in endothelial cells across different locations and pericyte phenotypes are distributed along the vascular tree [13]. This spatial heterogeneity is necessary for local NVC and functional hyperemia. However, it is still unclear whether CBF response patterns depend solely on cell types or also on spatial location. Therefore, understanding the CBF responses triggered at various locations by different neuron types can provide more insights into the relationship between brain activity and the vascular network.

Traditional optical stimulation is applied to the cerebral cortex using optical fibers [14,15]. Although this method is straightforward and easy to implement, it lacks flexibility in adjusting the position of the illumination spot, making it challenging to study heterogeneity. In addition, the fiber may obstruct part of the field of view (FOV). Another method involves using mirrors in combination with a scanning stage to move the mouse's position, thereby achieving photostimulation of different cortical sites [16]. There are studies focusing with an objective lens to reduce the size of light spots [11]. However, these methods lack flexibility in adjusting the position and size of the light spot. Wavefront modulation by Spatial Light Modulator (SLM) can achieve precise control over the size and position of the light spot, as well as enable rapid switching at different spatial locations [17]. This flexibility has not been fully utilized in previous studies, especially for local blood flow responses induced by different neurons. Additionally, beyond advancements in illumination techniques, real-time monitoring of blood flow changes is also invaluable for studying hemodynamic variations. Methods for detecting local hemodynamic response include laser doppler flowmetry (LDF) [18], functional magnetic resonance Imaging (fMRI) [10], optical intrinsic signal Imaging (OSI) [19], and laser speckle contrast imaging (LSCI) [9]. Among them, LSCI offers a non-contact, wide-field, and high-resolution method for relative blood flow measurement [20]. These advantages make LSCI a powerful tool for real-time, wide-field blood flow imaging [21].

In this study, we examined the effects of excitatory and inhibitory neuron activity on local CBF responses across different locations. Most excitatory signals are mediated by glutamate receptors, while inhibitory signals are primarily mediated by GABA receptors [22]. Therefore, our study used ChR2-labeled vesicular glutamate transporter 2 (VGLUT2) transgenic mice (VGLUT2-ChR2) and ChR2-labeled vesicular GABA transporter (VGAT) transgenic mice (VGAT-ChR2). Building on our previous work, which focused on high-resolution, real-time blood flow monitoring and spatially targeted photothrombosis [23], we extended its capability to precisely control the frequency, duty cycle, and duration of light stimulation using SLM. We applied different durations of optogenetic stimulation to the sensorimotor cortex of mice, and used LSCI to monitor real-time changes in local cerebral blood flow. By comparing the CBF responses induced by different types of neurons under various conditions, we analyzed their spatiotemporal characteristics to elucidate the distinct patterns of different neuron types in NVC.

2. Materials and methods

2.1. Animals and surgery

A total of 22 male and female mice, aged 2 to 4 months old and weighing 20 to 30 g, were used for experiments. Ten transgenic VGLUT2-ChR2-YFP were acquired by hybridizing VGLUT2-ires-Cre mice (Stock No.028863) and ChR2(H134R)-EYFP mice (Stock NO.024109)

Biomedical Optics EXPRESS

from the Jackson Laboratory (hereinafter referred to as VGLUT2-ChR2). Additionally, nine transgenic VGAT-ChR2-YFP (Stock No. 014548, Jackson Laboratory, hereinafter referred to as VGAT-ChR2) were used for photoactivation experiments. Three C57BL/6JNifdc (Charles River, China) mice were used for control experiments. All procedures involving animals were approved by the Hubei Provincial Animal Care and Use Committee and the Animal Experimentation Ethics Committee of Huazhong University of Science and Technology, China. Mice were kept under a standard 12 h light/dark cycle with free access to food and water.

The experimental animals were anesthetized using isoflurane in oxygen, with a concentration of 2% for induction and 1% to 1.5% for maintenance. A heating pad, controlled by a rectal thermometer (RWD, China), was employed to maintain the body temperature of the mice within the range of 36.8°C to 37°C. Following the exposure and saline cleansing of the skull, a craniotomy was conducted above the somatosensory cortex, ensuring the preservation of the dura [24]. A 1.5% agarose solution in HEPES-buffered artificial cerebrospinal fluid (pH 7.3) was applied to the exposed cortical surface at a temperature of 37°C [25]. Subsequently, a glass coverslip (diameter 6 mm) was placed over the cortical surface. For the duration of the optogenetic stimulation experiment, the anesthetic was transitioned to a combination of ketamine and xylazine at dosages of 100 mg/kg and 10 mg/kg, respectively. After the experiments, the mice were euthanized by intraperitoneal injection of pentobarbital at a dose of no less than 100 mg/kg.

2.2. Imaging system

The imaging system is shown in Fig. 1(a), which is similar to our previous report [23]. LSCI was performed using the red laser (He-Ne laser, 632.8 nm, 15 mW, Thorlabs, USA) which illuminated the cortical window at a perpendicular angle. The reflected light from cover glass is eliminated by polarization beam splitter (PBS251, Thorlabs, USA). The scattered light was relayed to a CCD camera (TXG14f, Baumer, Germany) for real-time blood flow imaging. Images were acquired at 30 frames per second with an exposure duration of 30 ms. Simultaneously, the laser modulated by the SLM (P1920-0523 HDMI; Meadowlark Optics, America) was delivered to the cortical window for spatially targeted optogenetic stimulation. We selected a 473 nm laser (MSL-FN-473/100, 100 mW, Changchun New Industries, China) and regulated its intensity using a continuous neutral density filter (NDC-50C-2, Thorlabs, USA).

The position, shape, and size of the illuminated spot are controlled through phase map, as shown in Fig. 1(b). The phase map was calculated from target illumination patterns by Gerchberg-Saxton (GSW) algorithm using MATLAB (2017a, MathWorks, USA) [17,23]. This calculated phase map is subsequently uploaded onto the SLM, which produced the desired diffraction pattern in conjunction with a Fourier lens (f = 200 mm; LA1708, Thorlabs, USA). The SLM's short edge measures 10.7 mm, and the Airy disk diameter under 473 nm light is about 22 μm. Although 84% of the Airy disk's energy is concentrated, the remaining 16% could still impact the experiment at the focal point. To fully block the zero-order spot and its diffraction, we used a block with a 1 mm diameter absorptive flat at its center. Then the patterned light travelled through the dichroic mirror (Di03-R473-t1-25 × 36, Semrock, USA) and the objective (PlanAPO, 1.25×, NA = 0.04, Olympus, Japan), thereby enabling spatially targeted optogenetic stimulation.

Optogenetic stimulation and real-time blood flow imaging were controlled by custom software written in the LABVIEW (LABVIEW 2013, National Instruments; U.S.). Compared to our previous study [23], we have achieved precise control over the frequency and duty cycle of the stimulation. The control of the loaded stimulation frequency was achieved by switching between the phase map and the isophase map. Additionally, the control of the stimulation pulse width was realized by adjusting the time ratio between the phase map and the isophase map loading.

Biomedical Optics EXPRESS

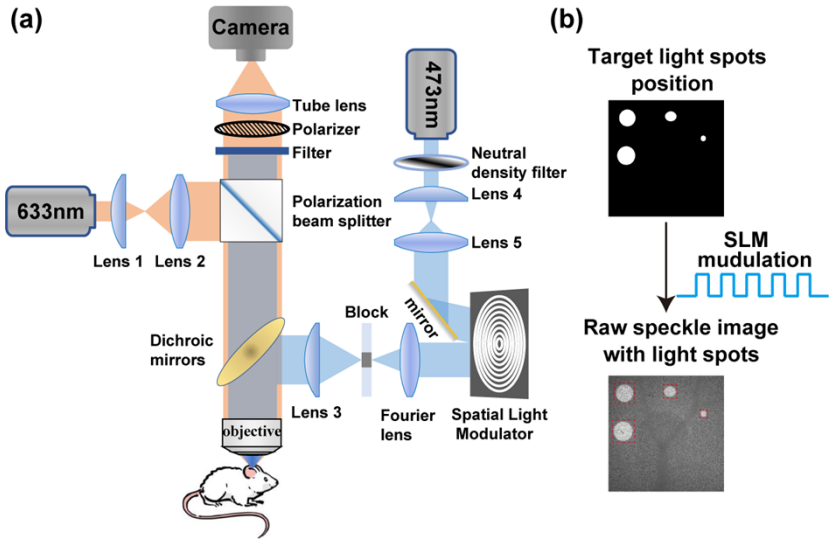

Fig. 1. Optogenetic stimulation and real-time blood flow imaging system. (a) Schematic diagram of the system. (b) The top image shows a binary map of manually selected target light spot positions, and the bottom image shows the original speckle image.

2.3. Optogenetic stimulation

Optogenetic stimulation frequency was set at 10 Hz with a 50% duty cycle. The diameter of the stimulation light spot was approximately 150 μm. The power under the objective lens was set to 0.2 mW for VGLUT2 and 0.5 mW for VGAT, enabling photostimulation to induce significant changes in CBF. Different numbers of pulses were used to achieve varying stimulation durations. The experiment employed 10, 20, 40, 60, 80, and 100 pulses, corresponding to light stimulation durations of 1s, 2s, 4s, 6s, 8s, and 10s, respectively. The baseline was recorded for 5 seconds prior to photostimulation. For 6-10s experiments, a total of 60s was recorded, while for other experiments, 25s was recorded. Three trials were conducted for each stimulating parameter for each mouse. The order of these trials was completely randomized, so trials with different parameters were conducted in no specific sequence. After each experiment, the mice were allowed to rest for at least 2 minutes to ensure that CBF returned to a resting state.

2.4. Data and statistical analysis

All data were analyzed using MATLAB. We employed a spatiotemporal laser speckle contrast analysis, which was conducted over a $7 \times 7 \times 5$ pixel volume, to determine the speckle contrast ($K_{x,y}$). Subsequently, we derived the blood flow index (BFI), calculated as BFI = $1/K_{x,y}^2$ [26–28]. To investigate the CBF response of the cerebral cortex to photostimulation, we selected the 5-second data before photostimulation as the baseline (BFI_b) and calculated the percentage change in CBF during the imaging period ($\Delta BFI/BFI_b \times 100\%$). In the following text, the curves represent the relative changes in CBF at the photostimulation site. The peak BFI indicated the maximum change in CBF. The time to peak referred to the duration from the start of recording to the peak BFI. The full width at half maximum (FWHM) represented the width at half of the peak BFI. The time to baseline indicated the duration from the start of recording until the CBF increases and then returns to baseline. Peak 2 indicated the maximum change observed during the second rise in CBF following an initial drop in bimodal pattern. The trough BFI represented the minimum value when the CBF drops below baseline in biphasic pattern. The interval between peaks refers to the time gap between the primary peak and either peak 2 or the trough.

Biomedical Optics EXPRESS

Statistical analysis was performed using GraphPad Prism (GraphPad Software, San Diego, CA, USA). All the data were presented as mean ± SD. Statistical significance between two groups was determined using unpaired t-test, while comparisons among multiple groups were conducted using one-way analysis of variance (ANOVA) followed by Tukey's post hoc test. $p<0.05$ was considered as statistical significance.

3. Results

3.1. Optogenetic activation of cortical neurons increases local CBF

The BFI image of the sensorimotor cortex was obtained using spatiotemporal speckle contrast analysis, as shown in Fig. 2. As an example in VGLUT2-ChR2, an area approximately 150 μm in diameter without large blood vessels was selected as the light stimulation site (red solid dot in Fig. 2(a)). The relative CBF change at the stimulation site of three different mice was shown in Fig. 2(b). Both VGLUT2-ChR2 and VGAT-ChR2 mice, which express light-sensitive proteins, exhibited local CBF increases, with VGLUT2-ChR2 mice showing a 37.8 ± 2.8% increase and VGAT-ChR2 mice showing a 22.3 ± 1.2% increase, while C57 mice, which do not express light-sensitive proteins, showed no significant change in CBF under light stimulation. Figure 2(c) illustrated representative spatial distribution of relative BFI changes over time in VGLUT2-ChR2 mice upon photostimulation. The stimulation was performed at a frequency of 10 Hz, with a power of 0.2 mW and a duration of 1s. The results indicated that photostimulation induced a localized increase in CBF in mice expressing the ChR2 light-sensitive protein. Importantly, this increase in CBF was attributed to the photosensitivity of ChR2 rather than the thermal effects of the light irradiation.

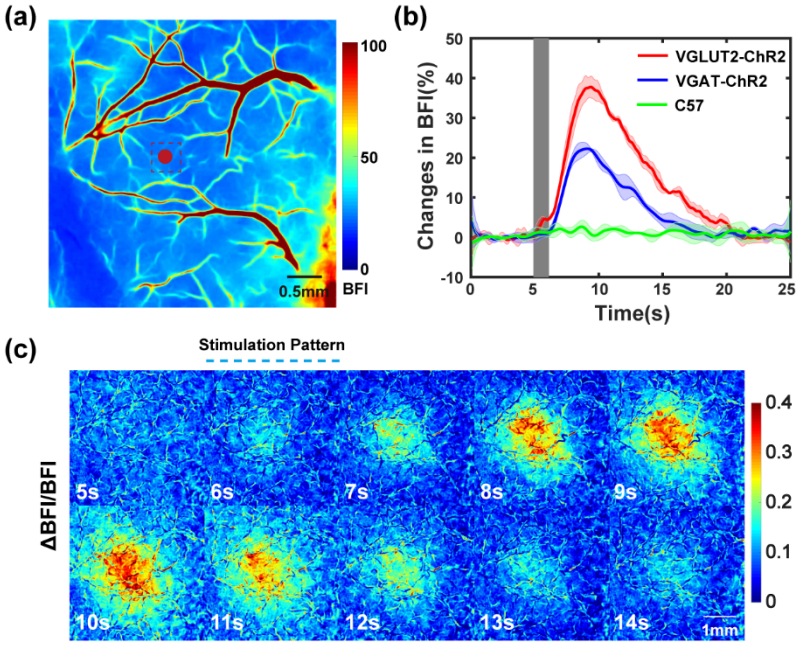

Fig. 2. Local CBF changes induced by photostimulation. (a) An illustration for BFI imaging of the sensorimotor cortex, with the red dot indicating the site of the photostimulation. (b) Relative changes in BFI at the photostimulation site (red dashed box in (a)) in VGLUT2-ChR2 mice (red line), VGAT-ChR2 mice (blue line), and C57 mice (green line). Gray box indicated photostimulation. (c) Representative images showing relative BFI change at different time points in VGLUT2-ChR2 mice.

Biomedical Optics EXPRESS

3.2. Three patterns of optogenetic-induced changes in local CBF

Photoactivation in either excitatory or inhibitory neurons lead to local BFI changes. In both VGLUT-ChR2 (Fig. 3(a)) and VGAT-ChR2 (Fig. 3(b)), BFI under photostimulation of different durations (stimulation duration:1-10s) exhibits a pattern of gradually increasing to a peak after the start of stimulation, followed by a slow decline. Compared to VGAT-ChR2 mice, VGLUT2-ChR2 mice exhibit a higher peak and longer duration in BFI changes. For instance, when the duration of stimulation was 8s, the peak BFI change in VGLUT2-ChR2 mice reached 58%, while it only reached 25% in VGAT-ChR2 mice. At 25s, the BFI in VGLUT2-ChR2 mice remains higher than that in VGAT-ChR2 mice. This difference may be related to the number of neurons and the regulatory effects of different neuron types on blood vessels, and a detailed comparison will be conducted subsequently. With shorter stimulation durations of 1-4s, CBF gradually returned to baseline within 25s. However, for longer stimulation durations of 6-10s, some CBF responses failed to return to baseline. This observation necessitated an extension of the monitoring period to 60 seconds to fully capture the dynamics of CBF. Three distinct patterns of CBF response were observed for longer stimulation durations: the unimodal pattern, the bimodal pattern, and the biphasic pattern.

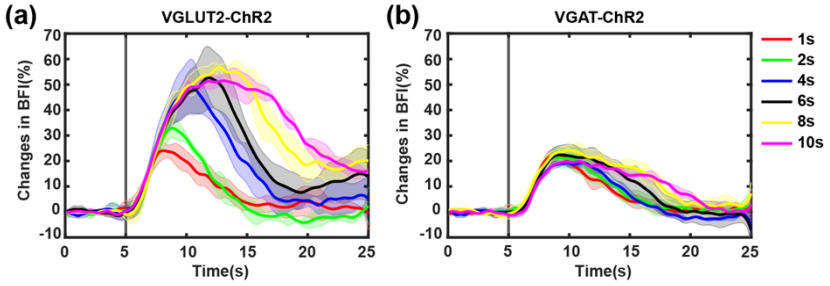

Fig. 3. Representative relative BFI changes over time at the photostimulation site under different durations of stimulation for excitatory and inhibitory neurons. (a) VGLUT2-ChR2 mice. (b) VGAT-ChR2 mice. The gray lines indicate the onset of photostimulation.

3.2.1. Unimodal pattern

In the unimodal pattern, following optogenetic stimulation, BFI rapidly increased to a peak, then began to slowly decline, and gradually returned to baseline (Fig. 4(a) and (b), using a stimulation duration of 6s-10s as an example). Both excitatory and inhibitory neurons exhibited this pattern of BFI change. For VGLUT2-ChR2, as the duration of light stimulation increased, the peak BFI also increased (from $19.9 \pm 8.8\%$ to $40.9 \pm 15.1\%$). When the duration exceeded 6 seconds, further increasing the stimulation duration did not significantly change the peak (Fig. 4(c), 8(s): $40.9 \pm 15.1\%$; 10s: $39.1 \pm 12.3\%$, $p > 0.05$). For VGAT-ChR2, the peak did not change much with increased stimulation duration (Fig. 4(c), 1(s): $14.8 \pm 5.1\%$; 10s: $17.2 \pm 3.2\%$, $p > 0.05$). As the duration of light stimulation increased, the peak BFI for VGLUT2-ChR2 increased by approximately 19.2% (Fig. 4(c), 1(s) vs. 10s), while for VGAT-ChR2, it increased by about 2.4% (Fig. 4(c), 1(s) *vs.* 10s). For stimulation durations of 2s or longer, the peak BFI for VGLUT2-ChR2 was significantly higher than for VGAT-ChR2 (all $p < 0.01$), indicating that excitatory neurons induced a significantly greater local CBF change than inhibitory neurons.

There was no significant difference in time to peak between the two types of neurons for the same light stimulation duration (Fig. 4(d), for example, 10s: 12.3 ± 2.5s *vs.* 11.3 ± 2.1s, all $p > 0.05$). The FWHM increased with longer stimulation durations. Only at 10s was the FWHM significantly greater for VGLUT2-ChR2 than for VGAT-ChR2 (Fig. 4(e), 13.7 ± 2.1s *vs.* 11.3 ± 2.2s, $p < 0.001$). The time to return to baseline also increased with longer stimulation

Biomedical Optics EXPRESS

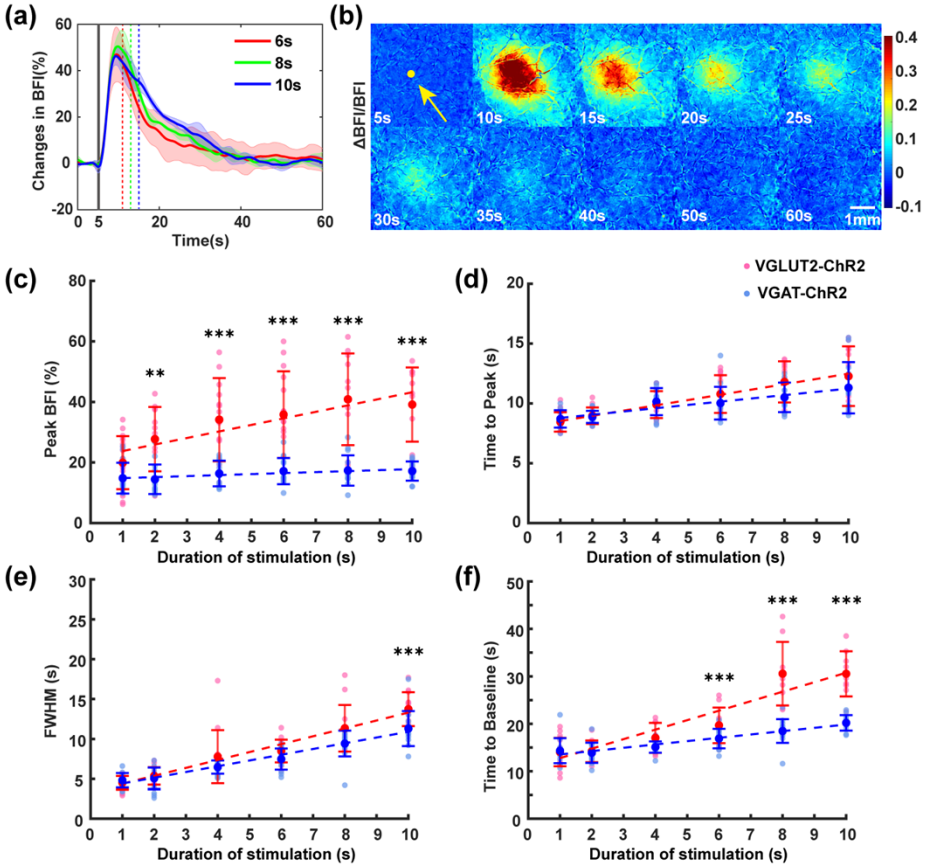

Fig. 4. Local CBF changes under different durations of stimulation in the unimodal pattern. (a) Representative relative BFI change curves induced by light stimulation durations of 6s, 8s, and 10s at the optogenetic stimulation site of VGLUT2-ChR2. The gray solid line indicates the onset of light stimulation, and the dashed lines indicate the end of light stimulation. Red: 6s; Green: 8s; Blue: 10s. (b) Representative relative BFI image of VGLUT2-ChR2 (10s light stimulation duration). The yellow dot marks the optogenetic stimulation site. (c-f) Response of optogenetic stimulation in the unimodal pattern for VGLUT2-ChR2 (red, n = 15) and VGAT-ChR2 (blue, n = 15) under different stimulation durations. (c) Peak BFI (y), red: $y = 0.00216t + 0.21627$, $R^2 = 0.23$; blue: $y = 0.00033t + 0.14515$, $R^2 = 0.05$. (d) Time to peak (y), red: $y = 0.43976t + 80.8853$, $R^2 = 0.49$; blue: $y = 0.27265t + 85.1501$, $R^2 = 0.32$. (e) FWHM (y), red: $y = 0.9905t + 33.9924$, $R^2 = 0.7$; blue: $y = 0.72043t + 36.9548$, $R^2 = 0.72$. (f) Time to baseline (y), $y = 1.9988t + 107.7218$, $R^2 = 0.69$; $y = 0.70056t + 128.4541$, $R^2 = 0.53$. Note: p value based on unpaired t-test between VGLUT2-ChR2 and VGAT-ChR2, $*p < 0.05$, $**p < 0.01$, $***p < 0.001$, n: experiments, t: stimulation duration, R^2: goodness of fit.

durations, and was significantly greater for VGLUT2-ChR2 than for VGAT-ChR2 at 6s, 8s, and 10s (Fig. 4(f), 19.7 ± 3.8s *vs.* 16.9 ± 2.1s, 30.6 ± 6.7s *vs.* 18.5 ± 2.5s, 30.5 ± 4.8s *vs.* 20.2 ± 1.6s, all $p < 0.001$). Overall, these results indicate that under the same light stimulation, excitatory neurons induced larger changes in CBF and took longer to return to baseline compared to inhibitory neurons.

Biomedical Optics EXPRESS

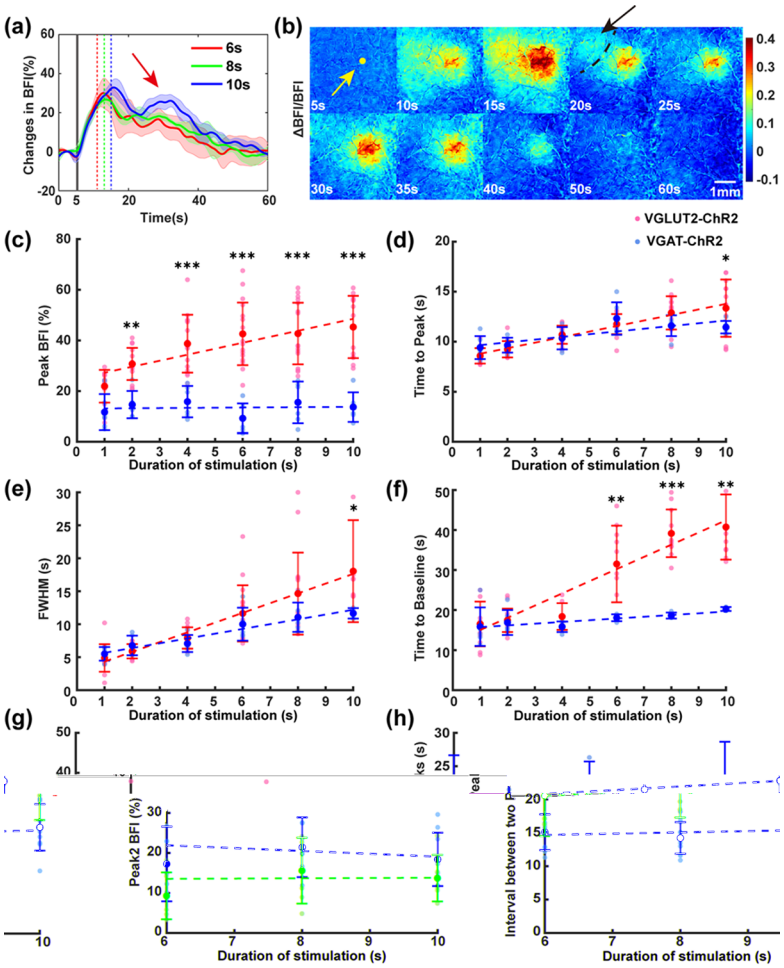

Fig. 5. Local CBF changes under different durations of stimulation in the bimodal pattern. (a) Representative relative BFI change curves induced by light stimulation durations of 6s, 8s, and 10s at the optogenetic stimulation site of VGLUT2-ChR2. The gray solid line indicates the onset of light stimulation, and the dashed lines indicate the end of light stimulation. Red: 6s; Green: 8s; Blue: 10s. The red arrow indicates the second peak. (b) Representative relative BFI image of VGLUT2-ChR2 (10s light stimulation duration). The yellow dot marks the optogenetic stimulation site. The black arrow points to the region with increased BFI not directly caused by light stimulation. (c-h) Response of optogenetic stimulation in the unimodal pattern for VGLUT2-ChR2 (red, n = 15) and VGAT-ChR2 (blue, n = 6) under different stimulation durations. (c) Peak BFI (y), red: $y = 0.00236t+0.2493$, $R^2 = 0.32$; blue: $y = 0.00007t+0.13105$, $R^2 = 0$. (d) Time to peak (y), red: $y = 0.55384t+82.4278$, $R^2 = 0.58$; blue: $y = 0.27292t+93.8712$, $R^2 = 0.35$. (e) FWHM (y), red: $y = 1.4784t+28.4992$, $R^2 = 0.53$; blue: $y = 0.72542t+49.3433$, $R^2 = 0.66$. (f) Time to baseline (y), $y = 3.0456t + 119.6247$, $R^2 = 0.71$; blue: $y = 0.43203t + 153.0343$, $R^2 = 0.2$. (g) Peak2 BFI (y), red: $y = -0.000711t + 0.26178$, $R^2 = 0.05$; blue: $y = 0.00007t + 0.13105$, $R^2 = 0$. (h) Interval between the two peaks (y), $y = 0.19225t + 135.3651$, $R^2 = 0.01$; blue: $y = 0.565t + 171.4154$, $R^2 = 0.04$. Note: p value based on unpaired t-test between VGLUT2-ChR2 and VGAT-ChR2, $*p < 0.05$, $**p < 0.01$, $***p < 0.001$, n: experiments, t: stimulation duration, R^2: goodness of fit.

Biomedical Optics EXPRESS

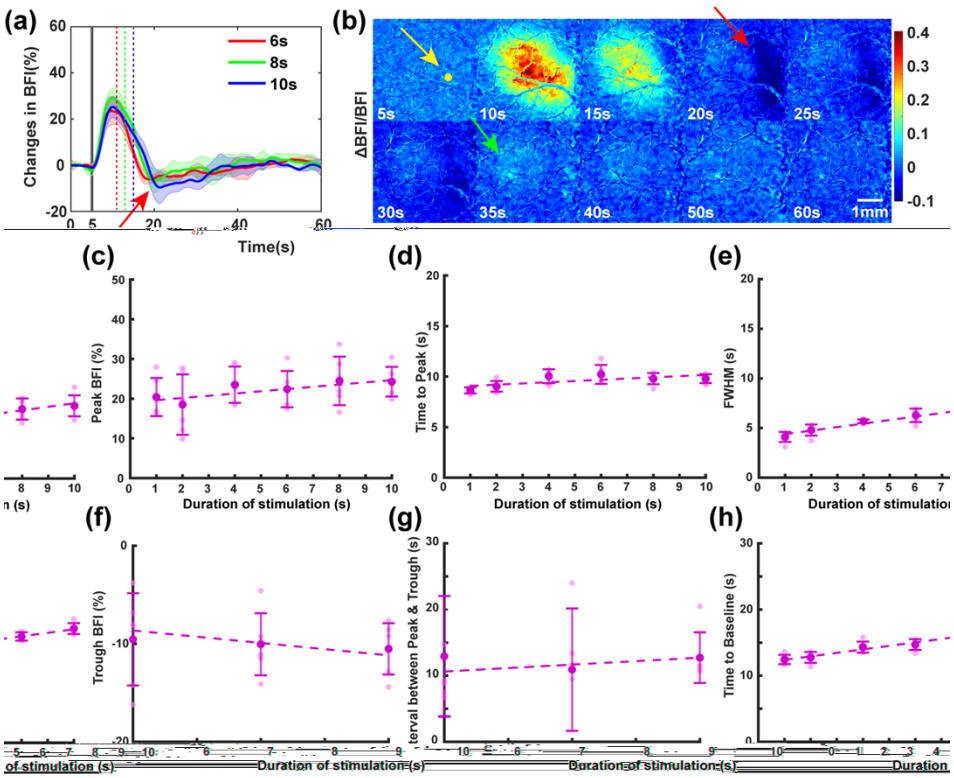

Fig. 6. Local CBF changes under different durations of stimulation in the biphasic pattern. (a) Representative relative BFI change curves induced by stimulation durations of 6s, 8s, and 10s at the optogenetic stimulation site of VGAT-ChR2. The gray solid line indicates the onset of light stimulation, and the dashed lines indicate the end of stimulation. Red: 6s; Green: 8s; Blue: 10s. The red arrow points to the area where BFI dropped below baseline. (b) Representative relative BFI image of VGAT-ChR2 (10s stimulation duration). The yellow dot marks the light stimulation site. The red arrow points to the area where BFI dropped below baseline, and the green arrow points to the area where BFI increased at non-stimulation sites. (c-h) Response of optogenetic stimulation in the unimodal pattern for VGAT-ChR2 (blue, n = 6) under different stimulation durations. (c) Peak BFI (y): $y = 0.00056t + 0.19365$, $R^2 = 0.11$. (d) Time to peak (y): $y = 0.12105t + 89.6068$, $R^2 = 0.24$. (e) FWHM (y): $y = 0.35507t + 40.3215$, $R^2 = 0.72$. (f) Trough BFI (y): $y = -0.000634t - 0.048411$, $R^2 = 0.33$. (g) Interval between peak & trough (y): $y = 0.52374t + 74.8288$, $R^2 = 0.09$. (h) Time to baseline (y): $y = 0.52758t + 118.6306$, $R^2 = 0.84$. Note: n: experiments, t: stimulation duration, R^2: goodness of fit.

3.2.2. Bimodal pattern

In the bimodal pattern, following light stimulation, BFI rapidly increased to a peak and then began to slowly decline. However, during the decline, a secondary rise occurred, reaching a second peak (red arrow in Fig. 5(a)) before gradually decreasing and returning to baseline (Fig. 5(a)). The relative BFI changes over time, as illustrated in Fig. 5(b), reveal that in the bimodal pattern, CBF alterations were not confined to the optogenetic stimulation region but also extended to non-stimulation sites (marked by black arrow in Fig. 5(b), left of the black dashed line). This suggested that the propagation of neuronal excitation may have led to increased CBF in distal non-stimulation regions, potentially causing the secondary rise in CBF at the optogenetic stimulation site. Beyond 6s, the peak did not change significantly for VGLUT2-ChR2 (red line in

Biomedical Optics EXPRESS

Fig. 5(c), 6(s): 42.6 ± 12.4%; 8s: 42.7 ± 12.2%; 10s: 45.3 ± 12.3%, p > 0.05). For VGAT-ChR2, the peak remained relatively constant with increased stimulation duration (1s: 11.7 ± 7.1%; 10s: 13.7 ± 5.8%). For stimulation durations of 2s or longer, the peak for VGLUT2-ChR2 was significantly higher than for VGAT-ChR2 (e.g., 2s: 30.8 ± 6.3% *vs.* 14.7 ± 5.4%, all $p < 0.01$).

As the duration of stimulation increased, the time to reach peak values tended to increase (e.g., 1s: 8.6 ± 0.8s *vs.* 4s 10.7 ± 0.9s, $p < 0.05$). However, when the time intervals were relatively short, no significant differences were observed (e.g., 8s: 12.9 ± 1.7s *vs.* 10s 13.4 ± 2.9s, $p > 0.05$). There was no significant difference in time to peak between the two groups for the same light duration except for the 10s (Fig. 5(d), all $p > 0.05$). The FWHM increased with longer stimulation durations (Fig. 5(e)). The time to baseline increased with longer light durations in VGLUT2-ChR2 (Fig. 5(f)), and was significantly longer for VGLUT2-ChR2 than for VGAT-ChR2 at 6s, 8s, and 10s (Fig. 5(f), 6(s): 31.5 ± 9.6s *vs.* 18.1 ± 0.9s, 8s: 39.2 ± 6s *vs.* 18.6 ± 0.8s, 10s: 40.7 ± 8.1s *vs.* 20.3 ± 0.5s, all $p < 0.01$). For the second peak, there was no significant change in both VGLUT2-ChR2 and VGAT-ChR2 peak2 BFI with the light duration increased (Fig. 5(g)). Finally, the interval between the two peaks did not change significantly with the duration of the stimulus; however, the interval in VGAT-ChR2 (blue line in Fig. 5(h)) was greater than that in VGLUT2-ChR2 (red line in Fig. 5(h)).

3.2.3. Biphasic pattern

The biphasic pattern was observed only in VGAT-ChR2. After photostimulation, BFI rapidly increased to a peak and then began to decline, dropping below baseline (red arrow in Fig. 6(a)) before gradually returning to baseline (Fig. 6(a)). Figure 6(b) showed the relative BFI changes over time for a 10s stimulation duration, with the red arrow pointing to the area where BFI at the optogenetic stimulation site fell below baseline. The biphasic pattern might have resulted from the excitation of inhibitory neurons, which suppressed the activity of neurons, ultimately causing a net decrease in CBF below baseline. Additionally, BFI increased in a surrounding area (green arrow at 35s in Fig. 6(b)). As shown in the scatter plots and fitted curves in Fig. 6((c)-(h)): the peak value increased from 20.4 ± 4.8% at 1s to 24.3 ± 3.7% at 10s; the time to peak gradually increased from 1s to 6s (1s: 8.6 ± 0.3s, 6s: 10.2 ± 0.9s), then decreased (8s: 9.8 ± 0.6s, 10s: 9.8 ± 0.4s); FWHM increased from 4.1 ± 0.5s at 1s to 7.3 ± 1.1s at 10s; the time to return to baseline increased from 12.5 ± 0.7s at 1s to 17.3 ± 0.8s at 10s. Overall, the parameters related to the peak gradually increased with longer stimulation durations, but the changes were not substantial. There was no significant difference in trough BFI as the stimulation duration increased. Due to the low goodness of fit, no conclusion can be made on the dependency of the trough BFI and the duration of stimulation (Fig. 6(f)).

In summary, photoactivation of both excitatory and inhibitory neurons initially resulted in a net increase in local CBF. However, after reaching the peak, the decline phase exhibited three different patterns across different locations. The most common pattern was the unimodal pattern, which occurred in approximately half of the experiments involving VGLUT2-ChR2 and VGAT-ChR2. The bimodal pattern featured a secondary peak during the CBF's gradual decline, albeit a lower one than the initial peak, and was observed in both VGLUT2-ChR2 and VGAT-ChR2. The biphasic pattern, characterized by a drop in CBF below the baseline during the return to baseline, leading to ischemia, was exclusive to VGAT-ChR2.

3.3. Spatial-specificity of local CBF

Through real-time blood flow imaging, high-resolution vascular distribution could be obtained. Cortical regions without blood vessels on the BFI image were selected for photostimulation, leading to varying stimulation locations across different experiments. As shown in Fig. 7(a), the photostimulation locations on the BFI image of the sensorimotor cortex were positioned based on the mouse skull edges and the bregma. Circles indicated VGLUT-ChR2 and squares indicated

Biomedical Optics EXPRESS

VGAT-ChR2, with different colors representing distinct CBF response patterns. According to Allen Mouse Common Coordinate Framework [29,30], Fig. 7(b) further illustrated the distribution of stimulation locations within functional brain regions. This indicates that even though optogenetic stimulation occurs within the sensorimotor cortex, the CBF response patterns may vary depending on the stimulation location.

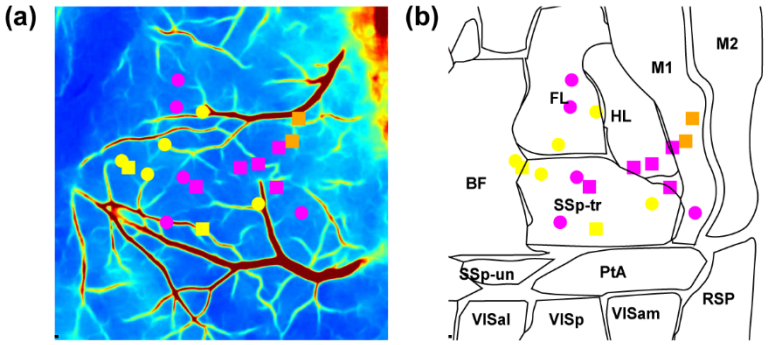

Fig. 7. Photostimulation locations. Magenta: unimodal Pattern; yellow: bimodal pattern; orange: biphasic pattern; circle: VGLUT-ChR2; square: VGAT-ChR2; (a) Typical BFI image. (b) Functional brain regions. (BF: Barrel field, SSp: Primary somatosensory, FL: Fore limb, HL: Hind limb, M1: Primary motor area, M2: Secondary motor area, PtA: Parietal association cortex, VIS: Visual area, RSP: Retrosplenial area).

We compared various parameters across different patterns in the same type of neurons, with the peak and time to peak in the bimodal and biphasic patterns both referring to the first peak. As shown in Fig. 8((a)-(c)), comparing the two patterns in VGLUT2-ChR2, there were no significant differences in peak value, time to peak, and FWHM (except at 10s) (all $p > 0.05$). This indicated that under the same duration of stimulation, the first peak in the bimodal pattern was similar to

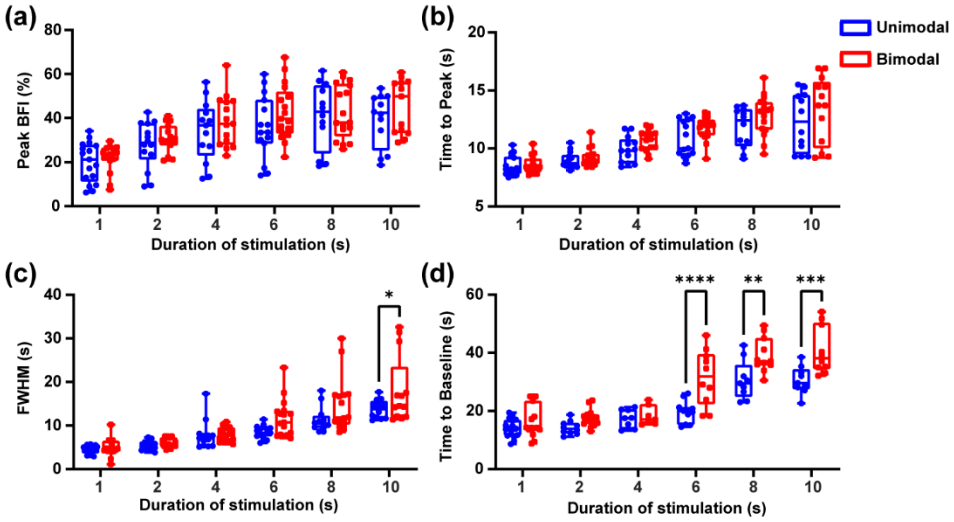

Fig. 8. Comparison of two patterns in VGLUT2-ChR2. (a) Peak value, (b) time to peak, (c) FWHM, and (d) time to return to baseline. Blue: Unimodal pattern, Red: Bimodal pattern. Note: p value based on unpaired t-test between unimodal and bimodal. *$p < 0.05$, **$p < 0.01$, ***$p < 0.001$, ****$p < 0.0001$.

Biomedical Optics EXPRESS

that in the unimodal pattern. However, the time to return to baseline was significantly greater in the bimodal pattern compared to the unimodal pattern at 6s, 8s, and 10s (Fig. 8(d), 6(s): 19.7 ± 3.8s *vs.* 31.5 ± 9.6s; 8s: 30.6 ± 6.7s *vs.* 39.2 ± 6s; 10s: 30.5 ± 4.8s *vs.* 40.7 ± 8.1s, all $p < 0.01$). The secondary increase in CBF not only slowed down decline but also extended the time required to return to baseline levels.

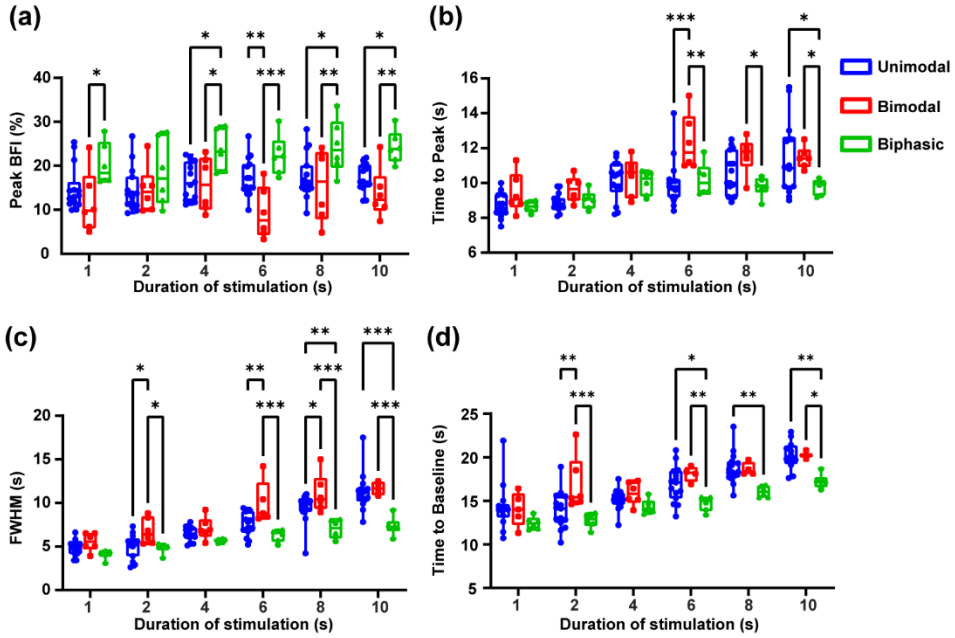

Fig. 9. Comparison of different patterns in VGAT-ChR2. (a) Peak value, (b) time to peak, (c) FWHM, and (d) time to return to baseline. Blue: Unimodal pattern, Red: Bimodal pattern, Green: Biphasic pattern. Note: p value based on one-way repeated-measures ANOVA followed by a post hoc Tukey's test. *$p < 0.05$, **$p < 0.01$, ***$p < 0.001$.

In VGAT-ChR2, there were no significant differences in peak value and time to peak between the unimodal and bimodal patterns (except at 6s) (Fig. 9(a) and (b), all $p > 0.05$). At 2s, 6s, and 8s, the FWHM was significantly greater in the bimodal pattern than in the unimodal pattern (Fig. 9(c), 5.1 ± 1.4s *vs.* 6.8 ± 1.5s; 7.5 ± 1.3s *vs.* 10 ± 2.5s; 9.4 ± 1.6s *vs.* 11.1 ± 2.2s, all $p < 0.05$), due to the tendency to form a second peak, which slowed the decline in BFI. The time to peak for the second peak in VGAT-ChR2 was longer than in VGLUT2-ChR2 (Fig. 5(d) and (h)), while the peak value in VGAT-ChR2 was significantly lower than in VGLUT2-ChR2, leading to a greater impact of the second peak on the FWHM in VGAT-ChR2. There was no significant difference in the time to return to baseline between the unimodal and bimodal patterns in VGAT-ChR2 (Fig. 9(d)). The peak values in the biphasic pattern (except at 2s) were significantly higher than those in the bimodal pattern (Fig. 9(a), e.g., 10s: 24.3 ± 3.7% *vs.* 13.7 ± 5.8%, all $p < 0.05$). In the biphasic pattern, the peak values at 4s, 8s, and 10s were significantly higher than those in the unimodal pattern (e.g., 8s: 24.5 ± 6.1% *vs.* 17.3 ± 5%, all $p < 0.05$). At stimulation durations of 6s, 8s, and 10s, the time to peak (Fig. 9(b), e.g., 10s: 9.8 ± 0.4s *vs.* 11.5 ± 0.6s, $p < 0.05$), FWHM (Fig. 9(c), e.g., 10s: 7.3 ± 1.1s *vs.* 11.7 ± 0.8s, $p < 0.001$), and time to return to baseline (Fig. 9(d), e.g., 10s: 17.3 ± 0.8s *vs.* 20.3 ± 0.5s, $p < 0.05$) in the biphasic pattern were significantly lower than those in the bimodal pattern.

Biomedical Optics EXPRESS

4. Discussion

In this study, we used optogenetic methods to investigate the spatiotemporal characteristics of local CBF changes induced by cortical excitatory (VGLUT) and inhibitory neurons (VGAT). The results revealed three patterns of local CBF changes induced by optogenetic stimulation. These patterns include an unimodal change, where CBF rapidly increases and then slowly returns to baseline; a bimodal change, where CBF rapidly increases, then slowly decreases, followed by a secondary rise before gradually returning to baseline; and a biphasic change, where CBF rapidly increases, drops below baseline, and then gradually returns to baseline. Activation of VGLUT neurons induced both unimodal and bimodal changes, while VGAT neurons induced unimodal and bimodal changes, as well as the unique biphasic change. These findings further support the spatiotemporal complexity of neurovascular coupling and highlight the importance of neuron-specific regulation in CBF dynamics.

The CBF response patterns of excitatory and inhibitory neurons differ in part, possibly due to their distinct mechanisms of interaction with blood vessels. In pyramidal cells, the activation of N-methyl-D-aspartate (NMDA) receptors stimulates the release of prostaglandin E2, produced by cyclooxygenase-2 (COX-2), leading to an increase in CBF [31–33]. For inhibitory neurons, signaling to blood vessels may occur through direct neurovascular connections, releasing neuropeptides and nitric oxide, thus affecting changes in CBF [34,35]. In the mouse neocortex, 70-80% of neurons are excitatory pyramidal neurons, while the remaining 20-30% are interneurons, most of which are inhibitory neurons [36]. VGLUT2-ChR2 excitation induces excitation in surrounding local neurons, whereas VGAT-ChR2 excitation induces inhibition in surrounding local neurons [37]. Therefore, the number of excitatory neurons stimulated by optogenetics is typically higher than that of inhibitory neurons, leading to further excitation of more neurons and requiring increased blood supply. In contrast, although inhibitory neurons also require energy, their activation suppresses local neuronal activity, reducing local energy demand. As a result, the peak values for excitatory neurons are significantly higher than for inhibitory neurons in both unimodal and bimodal patterns.

As the duration of stimulation increased, the peak BFI gradually rose and then stabilized. This was related to neurovascular regulation. With a light spot diameter of only 150 μm, the number of directly activated neurons was limited. As the stimulation time further increased, neural activity tended to saturate, and the peak of the blood flow changes no longer continued to increase. Research showed that short-term stimulation primarily caused arterial dilation, while long-term stimulation initiated arterial dilation, followed by increased capillary flow, and finally venous dilation [38,39]. Therefore, when neurons were continuously depolarized, the blood supply likely reached a local regulatory threshold, preventing further increases in the peak BFI. However, as the stimulation time extended, the FWHM and time to baseline also gradually increased, indicating that long stimulation maintained a hyperemic state to supply essential oxygen and energy for neural activity. The peak BFI changes in inhibitory neurons were less pronounced than those in excitatory neurons. This may be due to the smaller number of inhibitory neurons, which reached saturation with shorter-duration stimulation. It was also possible that sustained excitation of inhibitory neurons, further inhibited surrounding neurons [40], leading to a net effect on CBF changes that does not increase significantly. Our maximum stimulation duration was 10s. For subsequent studies, we can increase the intervals to further investigate changes in blood flow with longer stimulation durations.

For excitatory neurons, there were no significant differences in peak value, time to peak, and FWHM between unimodal and bimodal patterns, indicating that the CBF changes at the stimulation site due to photoactivation neurons are consistent. In the bimodal pattern, we observed increased local blood flow in regions adjacent to non-stimulated areas. This was likely due to the activation of excitatory neurons leading to the activation of surrounding neurons that were not directly stimulated, while inhibitory neurons suppressed the nearby inhibitory neurons, reducing

Biomedical Optics EXPRESS

their inhibitory effect on excitatory neurons [37]. This ultimately led to an increase in blood flow in the neighboring non-stimulated areas, triggering a secondary rise in CBF at the stimulation site. For the biphasic pattern in inhibitory neurons, the peak BFI and time to peak were significantly higher than those in unimodal and bimodal patterns. This suggests that the biphasic change might be due to the stronger inhibition of local cell activity by excited inhibitory neurons, causing the net effect on CBF to drop below baseline, resulting in ischemia. Regardless of whether the neurons were excitatory or inhibitory, the stimulation points were all located in the sensorimotor cortex. However, different CBF patterns were observed, highlighting the complexity of NVC and suggesting that there may be functional subunits within the sensorimotor cortex [41].

Each stimulation parameter was tested three times per mouse, yielding consistent blood flow responses. Therefore, we consider the CBF response pattern at the same location in the same mouse to be stable. Nevertheless, individual variability among mice, such as variations in the neuronal and vascular distribution of each mouse, particularly in vessel diameter [42], may influence the final blood flow response. In the future, increasing the number of stimulation sites and using additional landmarks like the lambda for precise positioning, along with considerations of vascular distribution, could allow for a more in-depth exploration of the relationship between stimulation sites and blood flow response patterns. Our system, with its ability to precisely control the location and range of photostimulation, holds significant potential for further research into the spatial specificity of CBF response patterns.

Our study primarily focuses on two types of neurons: excitatory (VGLUT2) and inhibitory (VGAT). Many studies have used Thy-1 in photoactivation experiments, typically resulting in an unimodal pattern [8,43]. Additionally, GABAergic neurons can be further divided into subtypes such as parvalbumin (PV), somatostatin (SOM), and vasoactive intestinal peptide (VIP). Research by Abe et al. demonstrated that activating PV neurons in the striatum led to a decrease in CBF [44]. Krawchuk et al. observed biphasic changes in CBF upon activating SOM neurons, whereas VIP neuron activation did not significantly alter CBF [18]. However, studies examining the effects of different stimulation durations on these neurons remained relatively limited and often used fiber-optic methods. Future research could explore in greater depth the spatiotemporal CBF response patterns of these neuron types.

By controlling the sites of photoactivation, it became easier to study functional connectivity across different brain regions. Previous methods often fiber or galvo scanner to achieve this illumination. Wu et al. used optical fiber illumination to inhibit transgenic mice, revealing a transcallosal effect of interneuron activation in the visual cortex [45]. Bauer et al. controlled the laser with 2D galvo scanner to irradiate different locations in the Thy-1-ChR2 mouse cortex, establishing an optogenetic functional connectivity map [46]. The adjustment of the optical fiber's illumination position can only be achieved manually, and it has a relatively large illumination range. Although a galvanometer scanner can change the illumination position by adjusting the angle, it also introduces a reflection angle and cannot control the size of the light spot. This limits the ability to control the range of light activation and the uniformity within the illuminated area. Our system utilizes wavefront modulation technology, enabling effective control of illumination at any position and within any range. Additionally, we can control the number of stimulation spots, allowing for simultaneous or sequential stimulation of multiple points. Our method is a powerful tool for studying interactions between different brain regions or across the cortex. Therefore, the whole-brain CBF response under optical activation will be a focus of our future research.

Our studies have several limitations. First, we used ketamine-xylazine anesthesia. Drew et al. found using two-photon imaging that anesthesia significantly weakened arterial responses to sensory stimulation and hindered venous dilation, indicating that anesthesia modulates CBF responses [38]. Dinh et al. discovered that when the mice were awake, the BOLD fMRI response was faster in all active regions and stronger in the subcortical areas compared with the anesthesia

Biomedical Optics EXPRESS

condition [47]. Although ketamine-xylazine can conserve the neurovascular relationship [48], the anesthetized state of the mice may affect hemodynamic responses. Abe et al. used optogenetic techniques to achieve CBF regulation in deep brain regions to study the relationship between CBF regulation and behavior [44]. Under anesthesia, it is impossible to study the effects of light modulation on behavior. Another limitation is the lack of direct monitoring of neural activity. Chen et al. directly monitored neural activity using brain electrodes, coupled with OCT, to study mathematical models of NVC [49]. Building on our method, multimodal systems that enable simultaneous monitoring of neuronal activity and hemodynamic changes hold significant potential. Such advancements would offer deeper insights into neuronal activity following optogenetic stimulation and support the exploration of spatial coupling between neurons and blood vessels.

5. Conclusion

By precisely controlling the position and size of the light stimulation and monitoring CBF with LSCI in real-time, this study identified different patterns of local CBF changes induced by excitatory and inhibitory neurons across different locations. Our results emphasize the importance of neuron type and spatial heterogeneity in neurovascular coupling and underscore our method's sophisticated capability to analyze the details of this complexity.

Funding. National Natural Science Foundation of China (82261138559, 62275095, 62275095); Hainan University Research Start-up Fund (KYQD(ZR)20072, KYQD(ZR)22074); CAMS Innovation Fund for Medical Sciences (2019-I2M-5-014); Science and Technology Innovation 2030- Major Project (No. 2022ZD0212200); Innovation Fund of WNLO.

Disclosures. The authors declare no conflicts of interest.

Data availability. Data underlying the results presented in this paper are not publicly available at this time but may be obtained from the authors upon reasonable request

References

1. T. L. Stackhouse and A. Mishra, "Neurovascular coupling in development and disease: focus on astrocytes.," Front. Cell Dev. Biol. **9**, 702832 (2021).
2. C. Iadecola, "The neurovascular unit coming of age: a journey through neurovascular coupling in health and disease," Neuron **96**(1), 17–42 (2017).
3. C. Iadecola, "The Pathobiology of Vascular Dementia," Neuron **80**(4), 844–866 (2013).
4. F. Atry, R. C. Chen, J. Pisaniello, *et al.*, "Optogenetic interrogation of neurovascular coupling in the cerebral cortex of transgenic mice," J. Neural Eng. **15**(5), 056033 (2018).
5. E. S. Boyden, F. Zhang, E. Bamberg, *et al.*, "Millisecond-timescale, genetically targeted optical control of neural activity," Nat. Neurosci. **8**(9), 1263–1268 (2005).
6. L. A. Gunaydin, O. Yizhar, A. Berndt, *et al.*, "Ultrafast optogenetic control," Nat. Neurosci. **13**(3), 387–392 (2010).
7. S. Zhao, J. T. Ting, H. E. Atallah, *et al.*, "Cell type-specific channelrhodopsin-2 transgenic mice for optogenetic dissection of neural circuitry function," Nat. Methods **8**(9), 745–752 (2011).
8. A. L. Vazquez, M. Fukuda, J. C. Crowley, *et al.*, "Neural and hemodynamic responses elicited by forelimb- and photo-stimulation in channelrhodopsin-2 mice: insights into the hemodynamic point spread function.," Cereb. cortex **24**(11), 2908–2919 (2014).
9. E. Anenberg, A. W. Chan, Y. Xie, *et al.*, "Optogenetic stimulation of GABA neurons can decrease local neuronal activity while increasing cortical blood flow.," J. Cereb. Blood Flow Metab. **35**(10), 1579–1586 (2015).
10. H. S. Moon, H. Jiang, T. T. Vo, *et al.*, "Contribution of excitatory and inhibitory neuronal activity to BOLD fMRI," Cereb. Cortex **31**(9), 4053–4067 (2021).
11. H. Uhlirova, K. Kılıç, P. Tian, *et al.*, "Cell type specificity of neurovascular coupling in cerebral cortex.," Elife **5**, e14315 (2016).
12. L. P. Bernier, C. Brunner, A. Cottarelli, *et al.*, "Location matters: navigating regional heterogeneity of the neurovascular unit," Front. Cell. Neurosci. **15**, 1 (2021).
13. M. Vanlandewijck, L. He, M. A. Mäe, *et al.*, "A molecular atlas of cell types and zonation in the brain vasculature," Nature **554**(7693), 475–480 (2018).
14. L. Ji, J. Zhou, R. Zafar, *et al.*, "Cortical neurovascular coupling driven by stimulation of channelrhodopsin-2.," PLoS One **7**(9), e46607 (2012).
15. B. Iordanova, A. Vazquez, T. D. Y. Kozai, *et al.*, "Optogenetic investigation of the variable neurovascular coupling along the interhemispheric circuits," J. Cereb. Blood Flow Metab. **38**(4), 627–640 (2018).

Biomedical Optics EXPRESS

16. O. G. S. Ayling, T. C. Harrison, J. D. Boyd, *et al.*, "Automated light-based mapping of motor cortex by photoactivation of channelrhodopsin-2 transgenic mice," Nat. Methods **6**(3), 219–224 (2009).
17. D. Wen, Y. Li, X. Zhu, *et al.*, "Selective photoactivation of neural activity combined with laser speckle imaging of cerebral blood flow," Opt. Lett. **43**(15), 3798 (2018).
18. M. B. Krawchuk, C. F. Ruff, X. Yang, *et al.*, "Optogenetic assessment of VIP, PV, SOM and NOS inhibitory neuron activity and cerebral blood flow regulation in mouse somato-sensory cortex," J. Cereb. Blood Flow Metab. **40**(7), 1427–1440 (2020).
19. L. Lee, L. Boorman, E. Glendenning, *et al.*, "Key aspects of neurovascular control mediated by specific populations of inhibitory cortical interneurons," Cereb. Cortex **30**(4), 2452–2464 (2020).
20. P. G. Vaz, A. Humeau-Heurtier, E. Figueiras, *et al.*, "Laser Speckle Imaging to Monitor Microvascular Blood Flow: A Review," IEEE Rev. Biomed. Eng. **9**, 106–120 (2016).
21. Z. Wang, W. Luo, F. Zhou, *et al.*, "Dynamic change of collateral flow varying with distribution of regional blood flow in acute ischemic rat cortex," J. Biomed. Opt. **17**(12), 125001 (2012).
22. S. Kantamneni, "Cross-talk and regulation between glutamate and GABAB receptors.," Front. Cell. Neurosci. **9**, 135 (2015).
23. X. Zhu, Z. Yi, R. Li, *et al.*, "Constructing a transient ischemia attack model utilizing flexible spatial targeting photothrombosis with real-time blood flow imaging feedback," Int. J. Mol. Sci. **25**(14), 7557 (2024).
24. T. H. Murphy, P. Li, K. Betts, *et al.*, "Two-photon imaging of stroke onset in vivo reveals that NMDA-receptor independent ischemic depolarization is the major cause of rapid reversible damage to dendrites and spines.," J. Neurosci. **28**(7), 1756–1772 (2008).
25. Y. Xie, S. Chen, E. Anenberg, *et al.*, "Resistance of optogenetically evoked motor function to global ischemia and reperfusion in mouse in vivo.," J. Cereb. Blood Flow Metab. **33**(8), 1148–1152 (2013).
26. D. D. Duncan and S. J. Kirkpatrick, "Spatio-temporal algorithms for processing laser speckle imaging data," in *Optics in Tissue Engineering and Regenerative Medicine II* 6858, 685802 (2008).
27. J. Qiu, "Spatiotemporal laser speckle contrast analysis for blood flow imaging with maximized speckle contrast," J. Biomed. Opt. **15**(1), 016003 (2010).
28. D. Briers, D. D. Duncan, E. Hirst, *et al.*, "Laser speckle contrast imaging: theoretical and practical limitations," J. Biomed. Opt. **18**(6), 066018 (2013).
29. E. S. Lein, M. J. Hawrylycz, N. Ao, *et al.*, "Genome-wide atlas of gene expression in the adult mouse brain.," Nature **445**(7124), 168–176 (2007).
30. J. M. Stafford, B. R. Jarrett, O. Miranda-Dominguez, *et al.*, "Large-scale topology and the default mode network in the mouse connectome.," Proc. Natl. Acad. Sci. U.S.A. **111**(52), 18745–18750 (2014).
31. A. Lacroix, X. Toussay, E. Anenberg, *et al.*, "COX-2-derived prostaglandin e2 produced by pyramidal neurons contributes to neurovascular coupling in the rodent cerebral cortex," J. Neurosci. **35**(34), 11791–11810 (2015).
32. C. Lecrux, X. Toussay, A. Kocharyan, *et al.*, "Pyramidal neurons are "neurogenic hubs" in the neurovascular coupling response to whisker stimulation," J. Neurosci. **31**(27), 9836–9847 (2011).
33. C. Lecrux and E. Hamel, "Neuronal networks and mediators of cortical neurovascular coupling responses in normal and altered brain states," Phil. Trans. R. Soc. B **371**(1705), 20150350 (2016).
34. B. Cauli, "Revisiting the role of neurons in neurovascular coupling," Front. Neuroenerg. **2**, 1 (2010).
35. Q. Perrenoud, J. Rossier, I. Férézou, *et al.*, "Activation of cortical 5-HT 3 receptor-expressing interneurons induces NO mediated vasodilatations and NPY mediated vasoconstrictions," Front. Neural Circuits (2012).
36. H. Markram, M. T. Rodriguez, Y. Wang, *et al.*, "Interneurons of the neocortical inhibitory system.," Nat. Rev. Neurosci. **5**(10), 793–807 (2004).
37. R. Tremblay, S. Lee, and B. Rudy, "GABAergic interneurons in the neocortex: from cellular properties to circuits," Neuron **91**(2), 260–292 (2016).
38. P. J. Drew, A. Y. Shih, and D. Kleinfeld, "Fluctuating and sensory-induced vasodynamics in rodent cortex extend arteriole capacity," Proc. Natl. Acad. Sci. **108**(20), 8473–8478 (2011).
39. C. T. Echagarruga, K. W. Gheres, J. N. Norwood, *et al.*, "nNOS-expressing interneurons control basal and behaviorally evoked arterial dilation in somatosensory cortex of mice," Elife **9**, 1–39 (2020).
40. X. Jiang, S. Shen, C. R. Cadwell, *et al.*, "Principles of connectivity among morphologically defined cell types in adult neocortex.," Science **350**(6264), aac9462 (2015).
41. M. Li, S. Gui, Q. Huang, *et al.*, "Density center-based fast clustering of widefield fluorescence imaging of cortical mesoscale functional connectivity and relation to structural connectivity.," Neurophotonics **6**(04), 1 (2019).
42. P. Padmanaban, A. Chizari, T. Knop, *et al.*, "Assessment of flow within developing chicken vasculature and biofabricated vascularized tissues using multimodal imaging techniques," Sci. Rep. **11**(1), 18251 (2021).
43. M. Böhm, D. Y. Chung, C. A. Gómez, *et al.*, "Neurovascular coupling during optogenetic functional activation: Local and remote stimulus-response characteristics, and uncoupling by spreading depression," J. Cereb. Blood Flow Metab. **40**(4), 808–822 (2020).
44. Y. Abe, S. Kwon, M. Oishi, *et al.*, "Optical manipulation of local cerebral blood flow in the deep brain of freely moving mice," Cell Rep. **36**(4), 109427 (2021).
45. W. Wu, L. Li, Y. Liu, *et al.*, "Modulation of visual responses and ocular dominance by contralateral inhibitory activation in the mouse visual cortex.," Int. J. Mol. Sci. **24**(6), 5750 (2023).

Biomedical Optics EXPRESS

46. A. Q. Bauer, A. W. Kraft, G. A. Baxter, *et al.*, "Effective connectivity measured using optogenetically evoked hemodynamic signals exhibits topography distinct from resting state functional connectivity in the mouse," Cereb. Cortex **28**(1), 370–386 (2018).
47. T. N. A. Dinh, W. B. Jung, H.-J. Shim, *et al.*, "Characteristics of fMRI responses to visual stimulation in anesthetized vs. awake mice," NeuroImage **226**, 117542 (2021).
48. M. A. Franceschini, H. Radhakrishnan, K. Thakur, *et al.*, "The effect of different anesthetics on neurovascular coupling," NeuroImage **51**(4), 1367–1377 (2010).
49. R. Chin-Hao Chen, F. Atry, T. Richner, *et al.*, "A system identification analysis of optogenetically evoked electrocorticography and cerebral blood flow responses," J. Neural Eng. **17**(5), 056049 (2020).